



# CHORUS

This is the accepted manuscript made available via CHORUS. The article has been published as:

## Measurement of Radiative Shock Properties by X-Ray Thomson Scattering

A. J. Visco, R. P. Drake, S. H. Glenzer, T. Döppner, G. Gregori, D. H. Froula, and M. J. Grosskopf

Phys. Rev. Lett. **108**, 145001 — Published 2 April 2012

DOI: [10.1103/PhysRevLett.108.145001](https://doi.org/10.1103/PhysRevLett.108.145001)

# Measurement of radiative shock properties by X-ray Thomson Scattering

A.J. Visco,<sup>1</sup> R.P. Drake,<sup>1</sup> S.H. Glenzer,<sup>2</sup> T. Döppner,<sup>2</sup> G. Gregori,<sup>3</sup> D.H. Froula,<sup>4</sup> and M. J. Grosskopf<sup>1</sup>

<sup>1</sup>*University of Michigan, Ann Arbor, MI 48109, USA*

<sup>2</sup>*Lawrence Livermore National Laboratories, Livermore, CA 94551, US*

<sup>3</sup>*University of Oxford, Oxford OX1 3PU, U.K.*

<sup>4</sup>*Laboratory of Laser Energetics, University of Rochester, Rochester, NY 14623 USA*

X-ray Thomson scattering has enabled us to measure the temperature of a shocked layer, produced in the laboratory, that is relevant to shocks emerging from supernovae. High energy lasers are used to create a shock in argon gas which is probed by x-ray scattering. The scattered, inelastic Compton feature allows inference of the electron temperature. It is measured to be 34 eV in the radiative precursor and  $\sim 60$  eV near the shock. Comparison of energy fluxes implied by the data demonstrates that the shock wave is strongly radiative.

The universe abounds with shock waves, from those driving the supernova (SN) explosions that create the elements of which life is made[1], to those crushing molecular clouds[2, 3], perhaps stimulating star formation, to those occurring when solid objects impact one another. In these shock waves radiative energy transfer significantly affects the structure and dynamics. Radiative shocks occur whenever shocks of sufficient velocity (typically some hundreds of km/s or more) are able to produce energetically significant fluxes of radiation. Shocks in supernovae trap radiation while traversing the star and then release it as they emerge [4]. Shocks in supernova remnants can be radiative both early [5], as they traverse dense matter left by stellar winds, and late [6, 7], when radiative cooling leads to large a compression of the shocked material. Colliding flows, for example in cataclysmic binary stars, can produce radiative shocks that either trap or release the radiation they produce, with consequences for the evolving morphology[8]. In this letter, we present the first demonstration from measurements that a laboratory shock wave is in fact strongly radiative.

Beyond measurements of shock velocity, nearly all previous radiative shock experiments have been limited to radiographic studies of their morphology[9, 10] or to measurements of the precursor (the heated material ahead of the shock)[11–15]. Some of this work [13] includes measurements of the effective temperature of shocked Xe from the emitted brightness. The signal in such measurements is dominated by emission from the dense, cool, post-shock Xe [16].

Here we use X-Ray Thomson Scattering (XRTS) [17] to probe shocked Ar, which cools more slowly than shocked Xe, enabling us to detect the presence of the hot post-shock matter and to directly infer from data that the shock is strongly radiative. XRTS has previously been applied to determine the plasma conditions in experiments studying inertial confinement fusion[18], isochoric heating[19], supersonic heat waves[20], and compressed warm dense matter[21, 22].

Here we describe how we demonstrate, from experimental laboratory data, that a shock is in fact strongly radiative, meaning that the structure of the shocked ma-

terial has been greatly altered by radiative emission. This demonstration proceeds as follows. The incident kinetic energy flux is  $E_k = \rho_o u_s^3/2$ , where the density of the unshocked material is  $\rho_o$  and the shock velocity is  $u_s$ . Under the assumption of local thermal equilibrium, the plasma emits a Planck spectrum modified by an emissivity. The total radiation energy flux leaving the two sides of the hot, shocked layer is  $E_R = 2\epsilon\sigma T_{es}^4$ , where the Boltzmann constant is  $\sigma$ ,  $T_{es}$  is the maximum value of the electron temperature  $T_e$ , and  $\epsilon$  is an effective emissivity. For a system to be in steady state, the incident kinetic energy must be enough to sustain the radiative energy, implying  $E_R \leq E_k$  and placing an upper limit on  $\epsilon$ . We infer from data below that for the energy fluxes to balance requires  $\epsilon \ll 1$  while the shocked material is also optically thick. This evidence implies that the shocked layer includes an optically thin, hot layer (which is the only way to make  $\epsilon \ll 1$ ) followed by lower-temperature material, and thus that the shock is strongly radiative[23].

The experiments used the Omega laser[24]. A  $20 \mu\text{m} \pm 20\%$  thick Be disk of  $\sim 2.5$  mm diameter is glued to an acrylic shock tube with an inner diameter of  $600 \pm 20 \mu\text{m}$ , filled with argon gas at 1.1 atm  $\pm 10\%$  (Fig. 1). Ten drive laser beams, of  $0.35 \mu\text{m}$  wavelength, each having 1 ns full-width at half-maximum (FWHM), flat-topped pulse duration with 100 ps rise and fall times, and equipped with  $11\text{\AA}$  smoothing by spectral dispersion [24] were focused, using distributed phase plates, into a  $820 \mu\text{m}$  spot (FWHM) on the Be disk. The average total energy delivered was  $3.9 \text{ kJ} \pm 1\%$ , producing a spatially averaged irradiance of  $7.4 \times 10^{14} \text{ W/cm}^2 \pm 3\%$ . These conditions ablate and accelerate Be plasma which in turn drives a shock in the radiative regime through the Ar gas at 100 -150 km/s, as previously measured using a streak camera [25]. The shock heats the ions to nearly 1 keV temperature, from simple estimates or simulations, leading to electron heating, further ionization, and copious radiation emission. An additional 8 laser beams of  $0.35 \mu\text{m}$  wavelength were focused onto a Mn dot to produce Mn He- $\alpha$  x-rays at 6.15 and 6.18 keV (see Fig. 1). The probe photons scattered by the plasma in the shock tube are spectrally resolved by a Bragg crystal spectrometer,

utilizing a highly-oriented pyrolytic graphite (HOPG) crystal in second diffraction order, coupled to a gated micro-channel plate with 180 ps gating time. The intersection of the probe beam x-rays and the projection of the window into the plasma define the scattering volume, the center of which is 3 mm from the Be disk. By varying the delay between the drive beams and the probe beams different parts of the system can be probed as the shock travels through the scattering volume. In the experiment, the probe beams were delayed by 19 ns or 15 ns in order to probe the dense region behind the shock interface or the ionizing precursor respectively. Measurement of scattered radiation from an undriven target shows that the probe radiation did not contribute to the inelastic spectra or significantly heat the plasma. The power of scattered

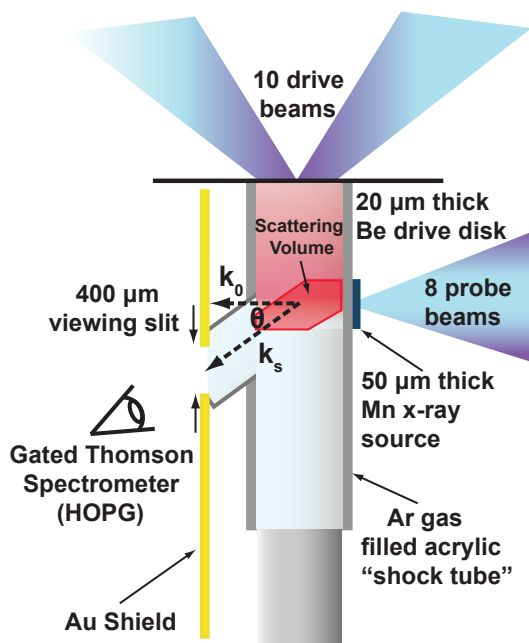


FIG. 1. Schematic of the experimental setup. Eight probe beams with 1 ns pulses, averaging 425 J, were focused onto a 500  $\mu\text{m}$  diameter Mn disk, placed 700  $\mu\text{m}$  from the tube axis, to produce probe x-rays which scatter from the shocked gas and are dispersed by a crystal spectrometer. A Au shield with a 400  $\mu\text{m}$  x 600  $\pm$  10  $\mu\text{m}$  viewing slit ensures that only light scattered through an angle of  $\theta = 79^\circ \pm 16^\circ$  reaches the spectrometer.

radiation arriving at the detector is proportional to electron number density times the dynamic structure factor:  $P_s(\mathbf{R}, \omega) \propto N S_{ee}^{tot}(\mathbf{k}, \omega)$ . [26] Here  $N$  is the total number of electrons, both bound and free, in the scattering volume. The dynamic structure factor is a measure of the correlations between scattering particles that give rise to the variation in scattered power as a function of the frequency. It was shown by Chihara [27] that contributions of bound and free electrons to the scattering processes could be separated and represented through the dynamic

structure factor:

$$S_{ee}^{tot}(\mathbf{k}, \omega) = |f(k) + q(k)|^2 S_{ii}(\mathbf{k}, \omega) + Z S_{ee}^0(\mathbf{k}, \omega) + S_{bf}(\mathbf{k}, \omega) \quad (1)$$

Here, the first term accounts for elastic scattering from electrons that follow the motions of the ions, both tightly bound, through the ion form factor  $f(k)$ , and those in the screening cloud around the ion, through  $q(k)$ . The ion structure factor,  $S_{ii}(\mathbf{k}, \omega)$ , represents the density correlations between ions. The contribution to the scattering by free electrons is given by the second term, where  $S_{ee}^0(\mathbf{k}, \omega)$  is the dynamic structure factor of free electrons and  $Z$  is the degree of ionization. The final term accounts for the inelastic scattering from bound electrons that are liberated into the continuum, and is negligible for the level of ionization ( $Z > 4$ ) corresponding to the temperatures observed in the radiative shock system. The signal of Eq(1) has elastic and inelastic (Compton in our case) contributions. We determined the shape of the elastic scattering spectrum, convolved with the response of our instrument, by measuring the spectrum of x-rays scattered from an undriven target, containing cold Ar gas. This is justified because inelastic scattering due to bound-free transitions from  $n=3$  electrons is 2 orders of magnitude smaller than elastic scattering in the cold Ar gas. The accuracy of this method depends on the reproducibility of the experiment. Calculations show that the error arising from the potential variability of the experimental configuration effects the measured temperature by  $\pm 5\%$

In Figure 2a we compare data from a measurement taken at 15 ns with the signal from an undriven target. Prominent in the data are the 6.15 and 6.18 keV scattering peaks due to near-elastic scattering from tightly bound electrons. Also in the data is the Cl Ly- $\alpha$  line (seen in 1st order at 2.96 keV) from the film the Mn backlighter was mounted upon. The photons scattered by the free electrons in the plasma are downshifted by  $\Delta E = \hbar^2 k^2 / 2m_e \pm \hbar \mathbf{k} \cdot \mathbf{v}$  to produce the inelastic feature. Here  $k = (2E_0 / \hbar c) \sin(\theta/2)$ , where  $E_0$  is energy of the probe radiation,  $\hbar$  is Planck's constant,  $m_e$  is the electron mass, and  $c$  is the speed of light. The first term is the result of Compton scattering,  $\hbar^2 k^2 / 2m_e \approx 60$  eV, determined by the geometry of the experiment and the energy of the probe. The second term represents the Doppler shift due to the photon scattering from an electron with a given velocity. Therefore the shape of the inelastic spectrum is a reflection of the velocity distribution of the free electrons. By subtracting the elastic signal from the total spectrum one can recover the inelastic spectrum, represented by the solid black line in Fig. 2a.

Since the electrons in our experiment are in the classical regime ( $T_e$  is  $\sim 55$  times the Fermi energy) the inelastic spectrum can be analyzed using the classical structure factor. Figure 2b shows the inelastic spectrum along with

theoretical spectra for various electron temperatures. At this time (15 ns) we expect the ionizing precursor to be in the scattering volume. The best fit shows that  $T_e$  is  $34 \text{ eV} \pm 14\%$ . For a delay of 19 ns, two scattering spectra were obtained from which  $T_e$  was determined to be  $60 \text{ eV} \pm 8\%$  and  $44 \text{ eV} \pm 11\%$ .

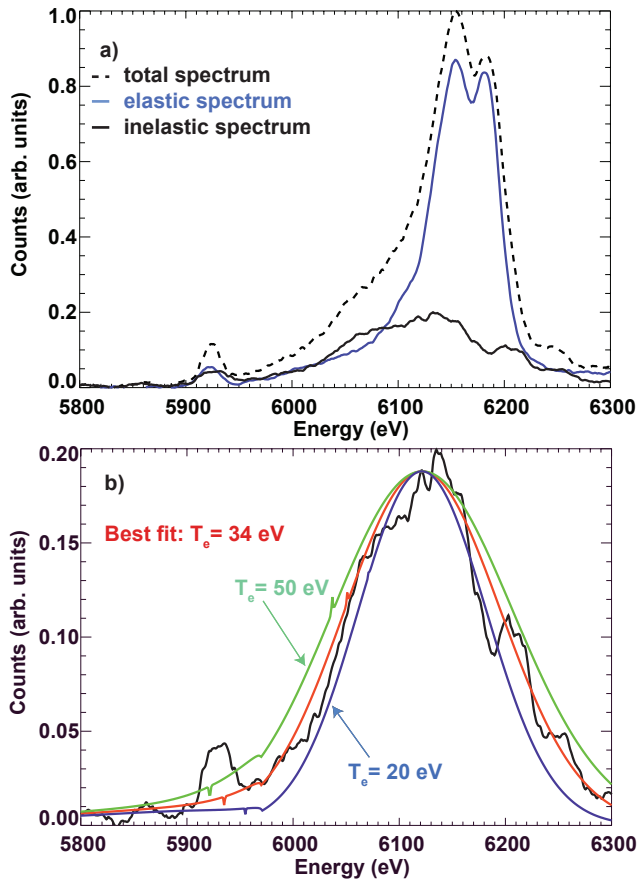


FIG. 2. a) Total scattered spectrum (dashed) for probe delayed 15 ns from drive beams plotted with elastic spectrum (blue) obtained from an undriven Ar target. The inelastic spectrum (black) is obtained by subtracting the elastic spectrum from the total spectrum. b) Inelastic scattering spectrum for a probe delayed 15 ns along with theoretical spectra for various electron temperatures. In both a) and b) the data are smoothed over a range of pixels corresponding to the spectral resolution of the instrument. (FWHM of source spectrum  $\sim 25 \text{ eV}$ ).

We note that  $T_e$  obtained in this way is essentially a measure of the second moment of the velocity distribution, and is a weighted average as described next. It only corresponds to an actual temperature when large regions of constant temperature are measured.

In the present system, the observed spectrum is the convolution of contributions from a range of conditions. To assess this effect, we simulated this system in 1D using the Hyades code, with an irradiance adjusted to match the observed shock position in prior experiments. Fig-

ure 3 shows results at both observation times. The red and blue lines show temperature and electron density respectively. We obtained the apparent temperature  $T_{eff}$ , represented by the green line, by convolving over the diagnostic window the local simulated  $T_e$  weighted by the local simulated electron density  $n_e$ . The weighting reflects the fact that the intensity of scattered radiation is proportional to the local electron density. At 15 ns the radiative precursor is probed. As the temperature and density don't vary appreciably through the scattering volume the calculated temperature is a reasonable measurement of the local temperature. At 19 ns the shock is expected to be in the scattering volume. The simulated local temperature  $T_e$  has its maximum at the shock front at  $T_{es} = 67 \text{ eV}$ . It is 33% larger than the maximum of  $T_{eff}$ , which is an average. Figure 3a shows a large variation in  $T_{eff}$  within the error range of the axial position due to the variability in the actual shock location from shot to shot, which explains the difference in the two temperature measurements at 19 ns.

From this perspective we take the averaged temperature of 60 eV as a lower limit for the maximum temperature in the scattering volume. Relying on the comparison of maxima in the simulations, we estimate the actual value of  $T_{es}$  to be 80 eV. The difference vs the simulated value may be due to overionization to  $Z \sim 11$  in the code, whose hydrogenic, average-atom ionization model does not account for the closed shell of Ne-like Ar at  $Z = 8$ . The high measured temperatures are due to the contribution from the hot, post-shock Ar that is cooling by radiation. In contrast, the emission temperature from a brightness measurement could be no larger than 45 eV, obtained by setting  $\epsilon = 1$  and  $u_s = 163 \text{ km/s}$ . This is an upper limit on the temperature of the cool, post-shock material. The simulation shown in Fig. 3 suggests that the actual value should be smaller, which is sensible because all the incoming energy is not converted to radiation. Referring to Figure 3, the scattering volume is much larger than the hot region of the shock. For the hot plasma to give a significant contribution to the scattered signal it must have considerably higher density than the precursor region, establishing that the dense region of the shock was probed.

It remains to evaluate the emissivity  $\epsilon$  as described above. Knowing the amount of mass swept up by the shock, and for a compression of 10 to 30, we find the optical depth at 60 eV to range from 4 to 7, so that  $\epsilon$  would be above 0.99 if the layer were at constant temperature. An upper limit for  $u_s$  is the average velocity of 163 km/s based on the location of the shock transition at the observation time. The actual velocity at the observation time will be significantly lower. This has been directly observed in experiments using Xe. For the present case, simulations suggest 138 km/s. For limiting values of  $u_s = 163 \text{ km/s}$  and  $T_{es} = 60 \text{ eV}$ , conservation of energy requires  $\epsilon \leq 0.16$ , while for the expected values

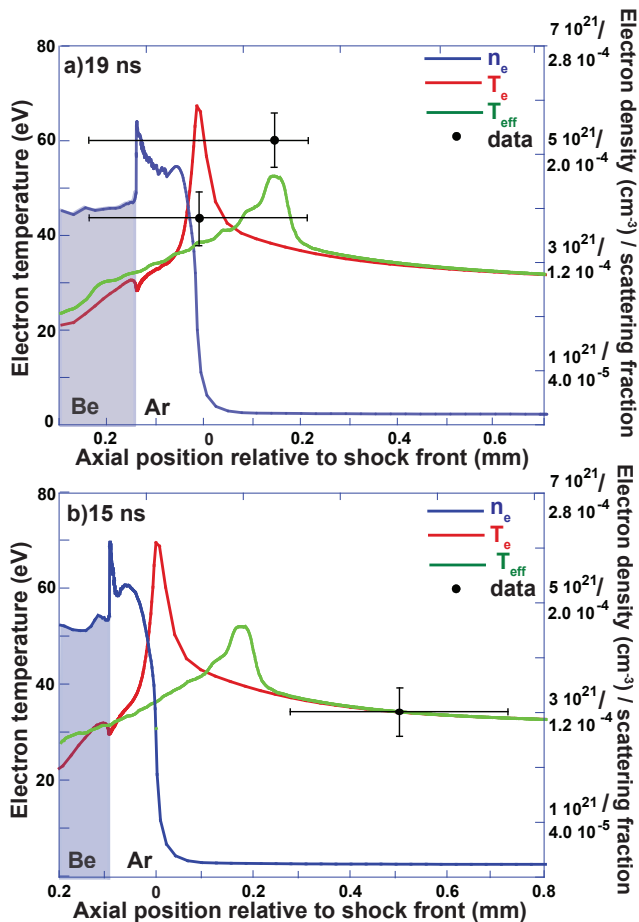


FIG. 3. Simulated profiles and data at 19 ns (top plot) and 15 ns (bottom plot), with regions of Be and Ar labeled. The blue and red curves show  $n_e$  and  $T_e$  as indicated. The scattering fraction is proportional to  $n_e$  and also follows the blue curve. The green curve is described in the text. The black dots are the measured temperatures, for both 19 and 15 ns data, located at the expected position of the viewing window. The uncertainty in this location with respect to the shock is taken to be  $225 \mu\text{m}$  based on the observed variability reported by Doss et al. [28] and the uncertainty in  $T_{eff}$  from the single-temperature fit. The right coordinates show both values of  $n_e$  and the fraction of the probe power scattered to the detector, with the latter obtained by averaging over scattering angle and solid angle with the assumption that these quantities and the polarization term do not vary axially.

of  $u_s = 138 \text{ km/s}$  and  $T_{es} = 80 \text{ eV}$ , we find  $\epsilon \leq 0.03$ . These calculations imply that the shock is strongly radiative, based on the argument explained at the start of this paper.

In summary, we have measured a weighted, averaged electron temperature in laboratory driven radiative shocks using XRTS. These measurements have enabled us to provide the first direct demonstration that these shocks are in the strongly radiative regime, allowing a more precise specification of the relation of these labora-

tory systems to astrophysical systems. This work lays the foundation for future XRTS experiments to measure the spatial profile of temperature, to ionization, and density.

This research was sponsored by the NNSA Stewardship Sciences Academic Alliances and the National Laser User Facility through DOE Research Grants DE-FG52-07NA28058 and DE-FG52-04NA00064, and by EPSRC grant No. EP/G007187/1 and Science and Technology Facilities Council of the United Kingdom. The work of S. H. G., and T.D. was supported by LDRD Grant No. 11-ERD-050 and was performed under the auspices of the U.S. Department of Energy by the Lawrence Livermore National Laboratory under Contract No. DE-AC52-07NA27344.

- [1] C. Chyba and C. Sagan, *Nature*, **355**, 125 (1992).
- [2] M. Maclow *et al.*, *ApJ*, **433**, 757 (1994).
- [3] G. Gregori *et al.*, *ApJ*, **527**, L113 (1999).
- [4] L. Ensmann and A. Burrows, *ApJ*, **393**, 742 (1992).
- [5] C. Fransson *et al.*, *ApJ*, **461**, 993 (1996).
- [6] J. M. Blondin *et al.*, *ApJ*, **500**, 342 (1998).
- [7] J. M. Laming and J. Grun, *Phys. Rev. Lett.*, **89**, 125002 (2002).
- [8] P. J. Armitage and M. Livio, *ApJ*, **493**, 898 (1998).
- [9] F. W. Doss *et al.*, *Phys. Plasmas*, **16**, 12705 (2009).
- [10] A. B. Reighard *et al.*, *Phys. Plasmas*, **13**, 082901 (2006).
- [11] S. Bouquet *et al.*, *Phys. Rev. Lett.*, **92**, 225001 (2004).
- [12] J. C. Bozier *et al.*, *Phys. Rev. Lett.*, **57**, 1304 (1986).
- [13] M. Koenig *et al.*, *Phys. Plasmas*, **13**, 056504 (2006).
- [14] T. Vinci *et al.*, *Phys. Plasmas*, **13**, 079903 (2006).
- [15] M. Busquet *et al.*, *High Energy Density Physics*, **3**, 8 (2007).
- [16] R. G. McClarren *et al.*, *Phys. Plasmas*, **17**, 093301 (2010).
- [17] S. H. Glenzer *et al.*, *Rev. Mod. Phys.*, **81**, 1625, (2009).
- [18] S. H. Glenzer *et al.*, *Phys. Plasmas*, **6**, 2117 (1999).
- [19] S. H. Glenzer *et al.*, *Phys. Plasmas*, **10**, 2433 (2003).
- [20] G. Gregori *et al.*, *Phys. Rev. Lett.*, **101**, 045003 (2008).
- [21] H. J. Lee *et al.*, *Phys. Rev. Lett.*, **102**, 115001 (2009).
- [22] A. L. Kritcher *et al.*, *Phys. Rev. Lett.*, **103**, 245004 (2009).
- [23] R.P. Drake, *High Energy Density Physics: Fundamentals, Inertial Fusion, and Experimental Astrophysics* (Springer, New York, 2006).
- [24] T. Boehly *et al.*, *Rev. Sci. Instr.*, **66** (1995).
- [25] A. J. Visco *et al.* to be published.
- [26] D. H. Froula, S. H. Glenzer, N. C. Luhmann, and J. Sheffield, *Plasma Scattering of Electromagnetic Radiation* (Academic Press, 30 Corporate Drive, Suite 400, Burlington, MA 01893, USA 2010).
- [27] J. Chihara, *Journal of Physics F: Metal Physics*, **17**, 295 (1987).
- [28] F. Doss, R. P. Drake, and C. C. Kuranz, in *High Energy Density Physics*, Vol. 6, ICHED - 2nd International Conference of High Energy Density Physics (Elsevier Science, 2009) pp.157-161